Available online at www.sciencedirect.com
SCIENCE DIRECT®
Combustion and Flame 141 (2005) 329–335
Combustion and Flame
www.elsevier.com/locate/combustflame

Fire dynamics simulation of a turbulent buoyant flame using a mixture-fraction-based combustion model

Y. Xin [a,1], J.P. Gore [a,*], K.B. McGrattan [b], R.G. Rehm [b], H.R. Baum [b]

[a] *School of Mechanical Engineering, Purdue University, West Lafayette, IN 47907-1003, USA*
[b] *National Institute of Standards and Technology, Gaithersburg, MD 20899-0001, USA*

Received 12 September 2002; received in revised form 15 June 2004; accepted 14 July 2004

Available online 14 August 2004

Abstract

Fire dynamics simulations of a 7.1-cm buoyant turbulent diffusion flame were performed using a mixture-fraction-based combustion model. In our previous work, good agreement between the measured and the calculated fire flow field was achieved with carefully selected domain and grid sizes using a Lagrangian thermal-element combustion model. The Lagrangian thermal-element model exhibits qualitative as well as quantitative differences in the measured and calculated temperature profiles in the flame zone. The number of Lagrangian thermal elements must be carefully selected and the model is not designed to provide insights into the species distributions in the fire. To address these issues, a mixture-fraction-based combustion model was used in the present work. The domain and grid size dependence using this model are documented. Comparisons between the measured and the calculated velocities, mixture fractions and temperatures show that the mixture-fraction-based combustion model captures the qualitative and quantitative fire behavior very well.

Keywords: Fire dynamics; Numerical simulations; Turbulent buoyant flames; Combustion models

1. Introduction

Accidental fires resulting from fuel spills and tank explosions commonly burn as pool fires. Numerical simulations of such fires can help safety designers reduce the associated hazards. The numerical simulations can be based on the Reynolds-averaged Navier–Stokes equations or the large eddy simulations (LES) or fire dynamics simulations (FDS) as reviewed recently by Novozhilov [1]. The LES and FDS methods capture the transient large-scale motion and intermittency of the buoyant fires. Motivated by these, Rehm and Baum [2] developed a special set of governing equations for fire simulations, which have been coded in the Fire Dynamics Simulator [3–6]. The FDS codes have been released for use by fire safety engineers [7,8].

In our previous work [9], FDS was evaluated using experimental data from a 7.3-cm-diameter helium plume and a 7.1-cm-diameter buoyant methane/air turbulent diffusion flame. The methane/air flame simulations utilized a Lagrangian thermal element model described in Ref. [7]. The computational results show that (1) the three-dimensional simulations are essential for capturing scalar and velocity distributions in

* Corresponding author. Fax: +1 765 494 0530.
E-mail address: gore@ecn.purdue.edu (J.P. Gore).
[1] Current address: FM Global Research, 1151 Boston–Providence Turnpike, Norwood, MA 02062, USA.

0010-2180/$ – see front matter
doi:10.1016/j.combustflame.2004.07.001

Nomenclature

B_i	Body force other than gravity in the ith direction (N/kg)
CFL	Courant–Friedrich–Levy number
c_{pi}	Specific heat (kJ/kg K)
D	Burner diameter (cm)
D_i	Diffusivity of species i (m^2/s)
g	Gravity (N/kg)
ΔH_o	Heat release per unit mass of oxygen consumed (kJ/kg)
H	Pressure-like term (m^2/s^2)
k	Thermal conductivity (m^2/s)
p	Pressure (Pa)
p_0	Background pressure, taken as 101,325 Pa
p_p	Perturbation pressure (Pa)
$\dot{q}'''$	Heat release rate (W/m^3)
q_r	Radiation heat flux (W/m^2)
ρ	Density (kg/m^3)
ρ_∞	Density of ambient air (kg/m^3)
T	Temperature (K)
t	Time (s)
u_j	The jth component of velocity (m/s)
x_j	Coordinate in the jth direction (m)
Y_i	Mass fraction of species i
Z	Mixture fraction
γ	Specific heat ratio
ε_{ijk}	Kronecker symbol, $\varepsilon_{ijk} = \begin{cases} 1, & ijk = 123, 231, 312, \\ -1, & ijk = 321, 213, 132, \\ 0, & \text{otherwise} \end{cases}$
ρ	Density (kg/m^3)
ρ_∞	Density of ambient air (kg/m^3)
τ_{ij}	Viscous stress (N/m^2)
$\bar{\phi}$	Spatial filtering of variable ϕ
$\tilde{\phi}$	Favre-averaged filtering of variable ϕ defined as $\bar{\rho}\tilde{\phi} = \overline{\rho\phi}$
ω_k	Vorticity in the kth direction (1/s)

the helium plume, particularly for the distances farther away from the source; (2) the fire-flow field can be calculated reasonably well with an adjustment of the time to burnout and with proper selection of the number of Lagrangian elements and the domain and grid sizes; and (3) there is qualitative agreement between the fire photographs and the contours of the highest temperature zone. The thermal element model involves release of notional parcels from the burner surface with the velocity of the fuel. There parcels release energy at a prescribed rate along their path when the burnout time elapses. Therefore, the behavior of a wrinkled laminar flame is not captured. As a result, the calculated peak temperatures in the persistent zone occur along the burner axis, where the maximum numbers of thermal elements reside. However, this is contrary to the experimental observation of a conical layer of the maximum temperature. Further, the Lagrangian model is not designed to provide insights into the species distributions in the fires. To address these problems, a mixture-fraction-based combustion model described in Ref. [8] was used in the present work. A comparison with the experimental data from this laboratory [10] shows excellent agreement between the two.

2. Experimental method

The flame is established on a diffuser burner with exit diameter $D = 7.1$ cm fueled by methane and burning in quiescent ambient air in an open environment [10]. The diverging angle of the burner is 7°, so the inflow is decelerated along the upward downstream direction and forms a top-hat velocity distribution of 3.14 cm/s at the burner exit. The fuel flow rate is selected to be 84.3 mg/s so that the calculated fire Froude number is 0.109 based on the definition given by Delichatsios [14], which matches that of a liquid toluene pool fire with the same pool size [10]. In calculating the fire Froude number, the radiation heat loss fraction estimated to be 10%, and the ambient temperature 288 K. Under the assumption of complete combustion, the total heat release rate of the fire is 4.2 kW and the visible flame height 36.4 cm.

The vertical and horizontal velocities were measured using particle image velocimetry and the species concentrations using gas chromatography by Zhou and Gore [10]. The measured species include CH_4, C_2H_2, C_2H_4, H_2, CO, O_2, and N_2. The mean temperature is calculated from the mean species concentrations, assuming an adiabatic flame with measured species concentrations, ignoring the effects of cross correlations between species, temperature, and specific heat. The mean mixture fraction was computed from the mean species concentrations based on its definition—the mass fraction of materials originated from the fuel stream. The fire photographs were taken for the same flame using a digital camera with 640 × 480 pixels. The calculated temperature contours were overlaid on the photographs corresponding to approximately the same phase in the puffing cycle of the fire (visually selected).

3. Governing equations

Following the work of Baum and his co-workers [2,7,8], the continuity, mixture fraction, and velocity divergence equations and ideal gas law need to be solved for buoyant turbulent fires. The key assumption in the derivation of these equations is that the pressure field in the fire can be decomposed into background pressure, hydrostatic pressure, and the pressure perturbation:

$$p(x_j,t) = p_0(t) - \rho_\infty g z + p_{\rm p}(x_j,t). \tag{1}$$

With this assumption, the pressure-related terms in the ideal gas law and the energy equation are only functions of time. However, the pressure term in the momentum equation is still a function of both time and space. The perturbation pressure in the momentum equation is solved using a Poisson equation,

$$\frac{\partial^2 H}{\partial x_j^2} = -\frac{\partial}{\partial t}\left(\frac{\partial u_j}{\partial x_j}\right) - \frac{\partial F}{\partial x_j}, \tag{2}$$

where H is defined as

$$\frac{\partial H}{\partial x_j} = \frac{1}{2}\frac{\partial}{\partial x_j}(u_i u_i) + \frac{1}{\rho}\frac{\partial p_{\rm p}}{\partial x_j} \tag{3}$$

and F is given by

$$F = -\varepsilon_{ijk} u_j \omega_k - \frac{1}{\rho}\left[(\rho-\rho_\infty)g + \frac{\partial \tau_{ij}}{\partial x_j} + \rho B_i\right]. \tag{4}$$

The velocity divergence in Eq. (2) is computed from

$$\frac{\partial u_j}{\partial x_j} = \frac{\gamma-1}{p_0\gamma}\left(\dot q''' + \nabla q_{\rm r} + \frac{\partial}{\partial x_j}\left(k\frac{\partial T}{\partial x_j}\right) + \frac{\partial}{\partial x_j}\left(\sum_i \rho c_{pi} T D_i \frac{\partial Y_i}{\partial x_j}\right) - \frac{1}{\gamma-1}\frac{dp_0(t)}{dt}\right). \tag{5}$$

Equation (5) is derived from the energy equation and the continuity equation under the assumption that nitrogen is the dominant species in the gas mixtures in the flame. The terms on the right-hand side represent contributions to velocity divergence by combustion heat release, radiative heat loss, heat conduction, enthalpy transport by diffusion, and background pressure change with time. For the present open-domain problem, the background pressure is assumed to be a constant of one atmosphere. Therefore, the pressure-related term vanishes in Eq. (5). The species concentrations in Eq. (5) are obtained using the laminar flamelet concept where the mixture fractions are solved from its conservation equation:

$$\rho\left(\frac{\partial Z}{\partial t} + u_j\frac{\partial Z}{\partial x_j}\right) = \frac{\partial}{\partial x_j}\left(\rho D\frac{\partial Z}{\partial x_j}\right). \tag{6}$$

In these governing equations, the turbulent stress τ_{ij}, turbulent heat and mass flux, combustion heat release rate $\dot q'''$, and radiation heat loss $q_{\rm r}$ are generally not resolved because the grids are relatively coarse compared to the Kolmogorov length scale (on the order of 1 mm) and flame surface thickness (<1 mm). To approximate the turbulent stress, the Smagorinsky model with a constant coefficient $C_{\rm s} = 0.2$ is used everywhere in the flow field. In this model, the viscosity is determined as the maximum of the molecular and the turbulent viscosities to reject unreasonably low or negative turbulent viscosity,

$$\mu_{\rm LES} = \max\left(\mu_{\rm molecular}, \rho(C_{\rm s}\Delta)^2|S|\right), \tag{7}$$

where Δ is the grid size and the mean strain rate S is calculated using the resolved velocity components:

$$|S|^2 = -\frac{2}{3}\left(\frac{\partial u_i}{\partial x_i}\right)^2 + \frac{1}{2}\left(\frac{\partial u_j}{\partial x_i} + \frac{\partial u_i}{\partial x_j}\right)^2. \tag{8}$$

The turbulent transport of heat and mixture fraction flux are approximated using prescribed $\mathrm{Sc} = 0.3$ and $\mathrm{Pr} = 0.5$. The radiative heat transfer plays a dominant role in large-scale fires. But for the weakly radiative laboratory-scale fire considered here, the radiation heat loss $\nabla q_{\rm r}$ is estimated to be 10% of the local combustion heat release rate $\dot q'''$, i.e., $\nabla q_{\rm r} = -0.1\dot q'''$. The combustion heat release rate $\dot q'''$ is very important in fire simulation because it causes the density differences resulting in the buoyancy forces that drive the fire flow field. In the present work, the combustion heat release rate $\dot q'''$ is estimated from a mixture-fraction-based combustion model.

4. Mixture-fraction-based combustion model

The basic assumption of the combustion model is that all the species mass fractions are only functions of the mixture fraction. Combining this assumption with the oxygen mass fraction equation and the further assumption of a single step forward chemical reaction, the heat release rate can be written as

$$\dot q''' = \Delta H_{\rm o}\rho D\left(\frac{\partial Z}{\partial x_j}\right)^2\frac{d^2 Y_{\rm o}}{dZ^2}. \tag{9}$$

In Eq. (9), $\Delta H_{\rm o}$ is the heat release per unit mass of oxygen that is consumed. It has been shown that this quantity is approximately equal for different types of fuels and therefore it is taken as 13,100 $\mathrm{kJ/kg_{O_2}}$ in the present study, as suggested by Huggett [11]. Equation (9) is valid only when the molecular diffusion process is fully resolved, which is usually not the case. Without the necessary grid resolution, Eqs. (1)–(5) provide only coarse approximations to the velocity, temperature, and species distributions.

These approximate solutions from FDS are similar to the filtered variables in the large eddy simulations. Denoting the coarse grid solutions to the density as $\bar{\rho}$ and the mixture fraction as $\tilde{Z}$, the approximate heat release rate can be written as

$$\dot{q}''' = \Delta H_o \bar{\rho} D \left(\frac{\partial \tilde{Z}}{\partial x_j} \right)^2 \left. \overline{\frac{d^2 Y_o}{dZ^2}} \right|_{\tilde{Z}=Z_{st}} . \quad (10)$$

In the model, it is assumed that the combustion occurs only in the vicinity of the stoichiometric mixture fraction Z_{st} because the grids spacing is larger than the flame thickness. Therefore, the neighboring cells at $\tilde{Z} = Z_{st}$ are located after solving the mixture fraction equation. In these cells, the approximate heat release rate is calculated using Eq. (10). The quantity $\bar{\rho} D (\partial \tilde{Z}/\partial x_j)^2$ is the scalar dissipation rate representing the diffusion of reactants into the flame surface. The quantity $\overline{(d^2 Y_o/dZ^2)}|_{\tilde{Z}=Z_{st}}$ scales the diffusion of reactants to yield the oxygen consumption rate. Naturally, the scalar dissipation rate and the scale factor for the oxygen consumption rate in Eq. (10) are approximate versions of the corresponding quantities in Eq. (9). The quantities $\bar{\rho} D$ and $\overline{(d^2 Y_o/dZ^2)}|_{\tilde{Z}=Z_{st}}$ are obtained from the state relationships, which are functional relationships between these quantities and the mixture fractions. The state relationships were based on opposed laminar flame calculations using OPPDIF [12]. The reaction mechanism included GRI-Mech 2.11 with 49 species and 279 elementary reactions [13].

5. Numerical considerations and boundary conditions

The governing equations are solved in the same order as listed above using a second order prediction and correction scheme. Once the velocity divergence is estimated from scalar variables using Eq. (5), the Poisson equation (Eq. (2)) is solved using the fast Fourier transform method [8]. Therefore, the numerical scheme is fully explicit. The pressure-like term H is then introduced into the momentum equation to update the velocity field. The local CFL number, defined using the maximum velocity magnitude in the entire flow field, the grid size, and the time step, is checked at this point and the time step is adjusted to ensure numerical stability if local CFL number is grater than unity.

The calculations were performed on a computational domain of $10 \times 10 \times 40$ cm. A uniform grid size of 2 mm is used over the domain to avoid commutation errors. This is approximately two times the estimated Kolmogorov length scale. Thus the molecular processes of diffusion and dissipation are not resolved in the present computations.

Two types of boundary conditions were used in the calculations: free boundary conditions on the surface of the open domain and prescribed velocity profiles at the fuel exit surface. Along the free boundaries, the values of the solution variables are equal to those next to them inside the computational domain if the velocity component normal to the boundaries is pointed outward. Otherwise, the values of the ambient air are assigned to the boundary grids. On the burner exit surface, a top-hat vertical velocity of 3.14 cm/s was prescribed based on the fuel flow rate and the burner geometry. Uniformly distributed random noise of 10% of the flow velocities was used for the initial conditions to mimic the upper stream disturbance.

6. Results and discussion

6.1. Instantaneous flame structures

Fig. 1 shows composites of two instantaneous fire photographs and the calculated temperature contours. When the two flame photos are compared, the instantaneous flame heights can vary significantly because of the unstable nature of the fire. The resemblance of the flame heights between the fire photos and the calculated temperature contours shows that the computations can reproduce this feature. The similarity in the shapes of the calculated temperature contours and the flame photographs in the multiple phase of the puffing cycle show the ability of the computations to capture at least qualitatively the underlying complex phenomena.

A comparison of measured and calculated instantaneous flow field further confirms this point, as

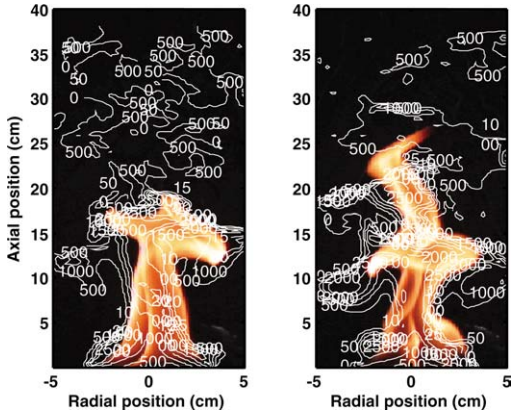

Fig. 1. A composite of fire photographs at two instants and the temperature contours (K) calculated by the FDS.

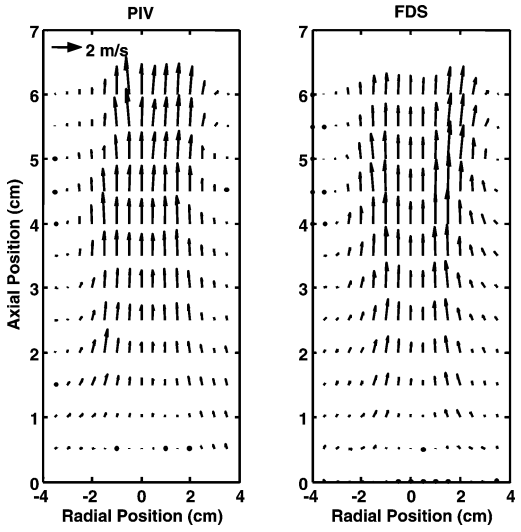

Fig. 2. A comparison of measured and calculated instantaneous velocity field.

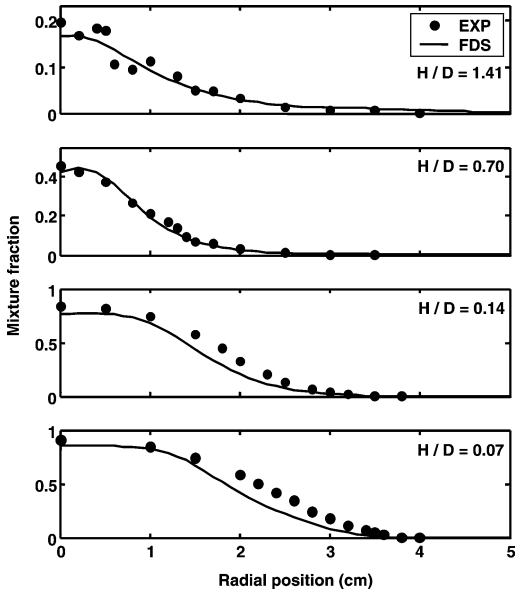

Fig. 3. Measured and calculated mean mixture fraction at different elevations above the burner exit.

shown in Fig. 2. The measured and calculated velocity vectors are similar to each other in both magnitude and directions. Within 6 cm from the burner exit, the flow is accelerated from 0.0314 m/s to about 1.5 m/s along the flame axis because of buoyancy. The ambient air is entrained to the fire through an annular region. The similarity between the measured and the calculated velocity fields validates the present simulations.

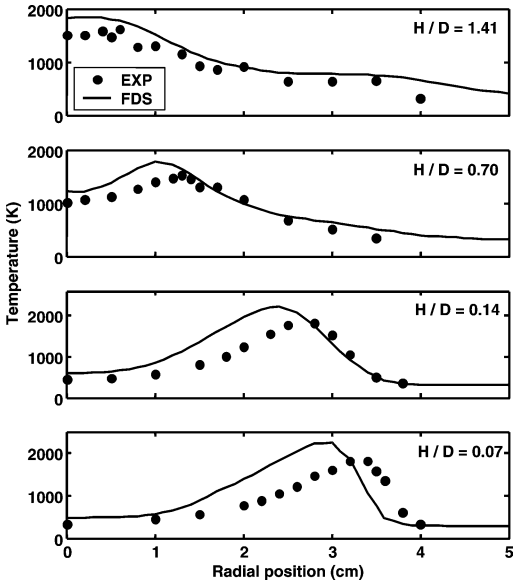

Fig. 4. Measured and calculated mean temperature at different elevations above the burner exit.

6.2. Ensemble-averaged scalars and flow field

An accurate prediction of the mixture fraction distributions is of critical importance because of its role in determining the heat release rate. Fig. 3 shows a comparison of the measured and calculated mean mixture fractions at four elevations above the burner exit. In Fig. 3 and the following figures, H/D denotes the ratio of the elevation above the burner to the burner diameter. The agreement between the measurements and the computations is excellent except for the slight underestimations between $R = 1.5$ and 3.5 cm at $H/D = 0.07$ and 0.14. The overall agreement strongly supports the applicability of the mixture-fraction-based combustion model.

Comparison of the measured and the calculated mean temperatures is shown in Fig. 4. The temperature distribution is calculated well at all four elevations. The mean flame surface positions are displaced toward the flame axis at the lower elevations. This discrepancy results in a relatively large error in the temperature estimates (∼500 K). The discrepancies are generally limited to the region near the burner exit. The temperature profiles at the farthest downstream locations are calculated reasonably well with the error less than 250 K.

Comparisons of the calculated and measured mean velocity components and a single mean vorticity component are shown in Figs. 5–7. The single vorticity component was computed based on the two ensemble-averaged velocity components. Fig. 5 shows that in general the vertical velocity is accurately estimated by the present models. At

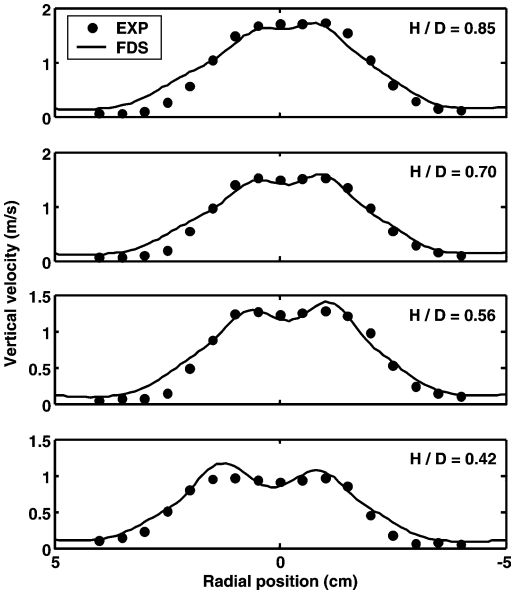

Fig. 5. Measured and calculated mean vertical velocity at different elevations above the burner exit.

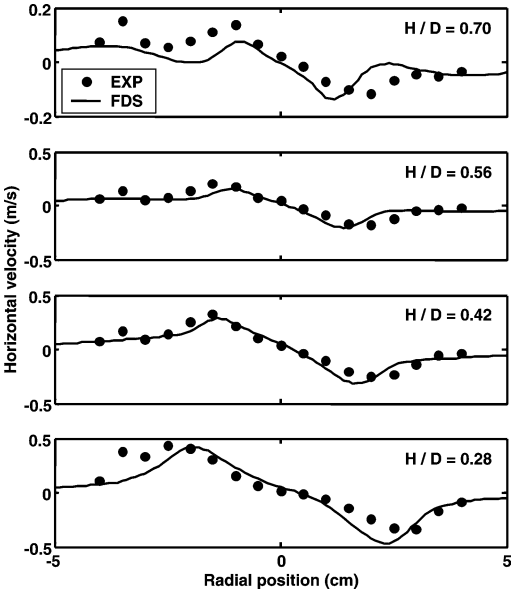

Fig. 6. Measured and calculated mean horizontal velocity at different elevations above the burner exit.

$H/D = 0.42$ and 0.56, slight discrepancies between the measured and the calculated vertical velocity exist near the burner axis. Because of the overestimation of temperature, a combination of the thermal expansion and buoyant forces leads to over acceleration of the flow. The overestimations result in discrepancies in the computed horizontal velocities near the flame surface as shown in Fig. 6. Along the flame

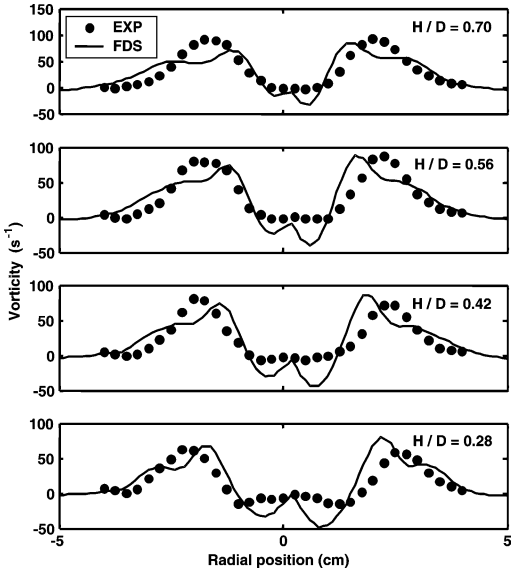

Fig. 7. Measured and calculated mean vorticity component at different elevations above the burner exit.

axis, the horizontal component of the velocity vector is accurately computed at all the flame elevations (Fig. 6) even though the vertical velocity is slightly underestimated (Fig. 5). This indicates that the FDS retains the ensemble-averaged axisymmetric nature of the fire. Using the two averaged velocity components, one component of the vorticity is computed. A comparison between measured and calculated vorticity (Fig. 7) shows that good agreement is achieved in the radial positions away from burner axis and flame surface. In the vicinity of these two regions, slight errors in the two velocity components are magnified resulting in the relatively large errors shown in Fig. 7. Taken together, the velocity and vorticity computations are in very good agreement with the measurements.

6.3. *Effects of the domain and grid sizes*

Effects of the domain and grid sizes are studied and the results for mean vertical velocities are shown in Figs. 8 and 9. In the domain size effect study, the domain sizes are increased by 50 and 100% from $10 \times 10 \times 40$ cm with a fixed grid size of 3.125 mm (Fig. 8). The results show the domain dependency of the calculated vertical velocities is very small for all four elevations. In the grid size effect study, the grid sizes are increased from 2 mm to 2.5 and 3.125 mm with a fixed domain size of $15 \times 15 \times 60$ cm. For all the elevations shown in Fig. 9, the grid effects are usually within 10%.

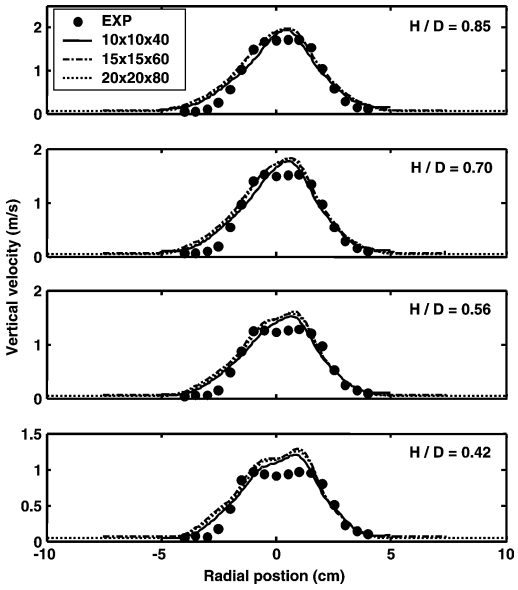

Fig. 8. Effects of domain size on mean vertical velocity at different elevations above the burner exit. The grid size is 3.125 mm for all three cases.

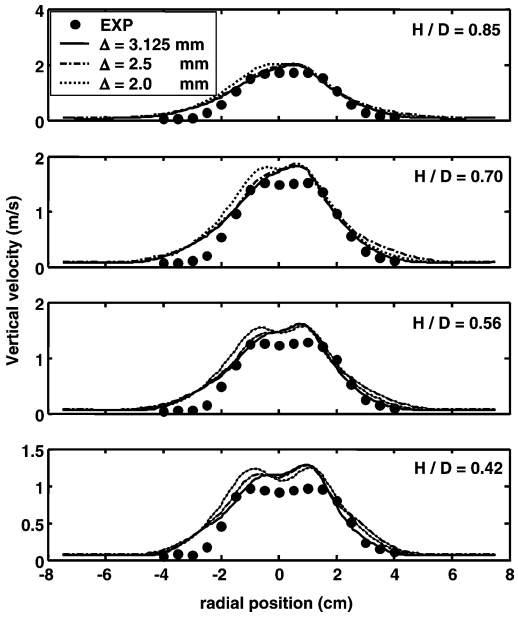

Fig. 9. Effects of grid size (Δ) on mean vertical velocity at different elevations above the burner exit. The grid size is $15 \times 15 \times 60$ cm for all three cases.

7. Conclusions

Fire dynamics simulations of a 7.1-cm buoyant turbulent diffusion flame were performed using a mixture-fraction-based combustion model. The results show that:

(1) FDS can qualitatively capture the instantaneous fire structures and quantitatively reproduces the averaged scalars and velocities.
(2) With the present methods, relatively small domain sizes and relatively coarse grid sizes yield simulations with reasonably small errors.
(3) The agreement between the measured and calculated mean values of mixture fractions, temperatures and velocities establishes the applicability of the mixture-fraction-based combustion model for buoyant flames.

Acknowledgment

This work at Purdue University is supported by the National Institute of Standards and Technology under Grant 60NANA9D0093, with Dr. Howard Baum and Dr. Anthony Hamins serving as NIST Scientific Officers.

References

[1] V. Novozhilov, Prog. Energy Combust. Sci. 21 (2001) 611–666.
[2] R.G. Rehm, H.R. Baum, J. Res. NBS 83 (1978) 297–308.
[3] K.B. McGrattan, R.G. Rehm, H.R. Baum, J. Comput. Phys. 110 (1994) 285–291.
[4] W.E. Mell, K.B. McGrattan, H.R. Baum, Proc. Combust. Inst. 26 (1996) 1523.
[5] H.R. Baum, W.E. Mell, Combust. Theory Model. 2 (1998) 405–422.
[6] K.B. McGrattan, H.R. Baum, R.G. Rehm, Fire Safety J. 30 (1998) 161–178.
[7] K.B. McGrattan, H.R. Baum, R.G. Rehm, A. Hamins, G.P. Forney, Fire Dynamics Simulator—Technical References Guide, Report NISTIR6467, National Institute of Standards and Technology, 2000.
[8] K.B. McGrattan, H.R. Baum, R.G. Rehm, A. Hamins, G.P. Forney, J.E. Floyd, S. Hostikka, Fire Dynamics Simulator—Technical Reference Guide, Version 2, Report NISTIR6783, National Institute of Standards and Technology, 2001.
[9] Y. Xin, J.P. Gore, K.B. McGrattan, R.G. Rehm, H.R. Baum, Proc. Combust. Inst. 29 (2002) 259–266.
[10] X.C. Zhou, J.P. Gore, Proc. Combust. Inst. 27 (1998) 2767.
[11] C. Huggett, Fire Mater. 4 (1980) 61–65.
[12] A.E. Lutz, R.J. Kee, J.F. Grcar, F.M. Rupley, OPPDIF: A Fortran Program for Computing Opposed-Flow Diffusion Flames, Report SAND96-8243, Sandia National Laboratories, 1996.
[13] C.T. Bowman, R.K. Hanson, D.F. Davidson, W.C. Gardiner Jr., V. Lissianski, G.P. Smith, D.M. Golden, M. Frenklach, M. Goldenberg, GRI-Mech 2.11, http://www.me.berkeley.edu/gri_mech/.
[14] M.A. Delichatsios, Combust. Flame 70 (1987) 33–46.